Koyama, D., Donaldson, P. M., & Orr-Ewing, A. (2017). Femtosecond to Microsecond Observation of the Photochemical Reaction of 1,2-di(quinolin-2-yl)disulfide with Methyl Methacrylate. *Physical Chemistry Chemical Physics*, *19*(20), 12981-12991. https://doi.org/10.1039/C7CP01784G

Journal Name

ARTICLE

Femtosecond to Microsecond Observation of the Photochemical Reaction of 1,2-di(quinolin-2-yl)disulfide with Methyl Methacrylate

Received 00th January 20xx,
Accepted 00th January 20xx

DOI: 10.1039/x0xx00000x

www.rsc.org/

Daisuke Koyama,[a] Paul M. Donaldson[b] and Andrew J. Orr-Ewing[a]

The mechanism of the thiol-ene reaction induced by 330-nm ultraviolet excitation of 1,2-di(quinolin-2-yl)disulfide (QSSQ) in the presence of methyl methacrylate (MMA) is investigated by sub-picosecond to microsecond transient absorption spectroscopy. The measurements, spanning more than seven orders of magnitude of time, directly reveal multiple radical reaction steps. The ground state quinoliene-2-thiyl radical (QS) is formed with a time constant of ~200 fs by photolysis of QSSQ, followed by (64 ± 1)% decay of the initially formed QS radical because of solvent cage induced geminate recombination and QS dimer formation with a rate coefficient of (3.4 ± 0.2) × 10^{10} M^{-1} s^{-1} in methanol solution. In MMA solution, the carbon centered radical QS-MMA forms with a bimolecular reaction rate coefficient of (2.8 ± 0.2) × 10^{7} M^{-1} s^{-1}. The distinct infrared band at 1653 cm^{-1} assigned to the C=O stretch mode of the QS-MMA radical decays rapidly in aerated solution, in contrast to observations in a solution purged of O_2 by N_2 bubbling. This decay is attributed to reaction of the QS-MMA radicals with molecular oxygen, producing peroxy radicals. Kinetic analysis of the intensity of the band at 1653 cm^{-1} reveals a bimolecular reaction rate coefficient of (3.3 ± 0.3) × 10^{9} M^{-1} s^{-1} for the reaction of the QS-MMA radicals with molecular oxygen, and indicates that this reaction step is reversible.

1. Introduction

Thiol-ene reactions, in which a thiyl radical reacts with alkenes or alkynes, have been studied for more than a century,[1] but the development of "Click-Chemistry" is inspiring new applications in synthetic and functional materials chemistry.[2] Thiol-ene reactions can be carried out under mild reaction conditions to yield new C-S bonds with high reaction selectivity and atom economy,[3, 4] and therefore have been proposed as a useful methodology for synthesis of functional molecules.[5, 6]

Thiol-ene reactions proceed *via* reaction steps (i) – (iii), but also potentially include other reaction steps (iv) – (vii), which result in side-products:[6, 7]

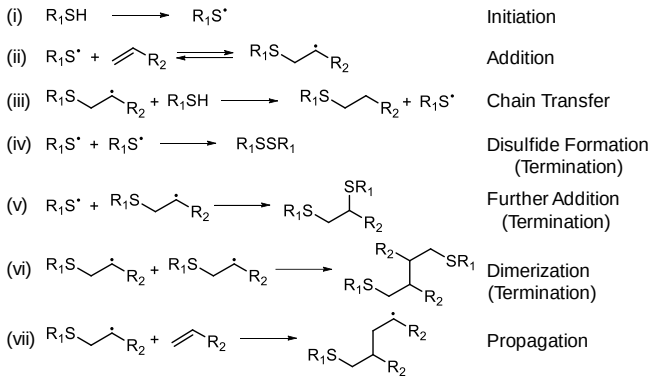

Light irradiation or radical initiators can be used to produce thiyl radicals (step (i)), but the former method involving photodissociation of the corresponding thiol (as shown in (i)) or disulfide is preferred for the study of their mechanisms and dynamics because of the almost instantaneous (sub-picosecond) formation of thiyl radicals.[8-10] The photodissociation dynamics producing aromatic thiyl radicals have mostly been deduced from studies using transient electronic absorption spectroscopy (TEAS),[8-17] because aromatic thiyl radicals show strong absorption bands in the ultraviolet (UV) and visible regions.[6] The mechanisms of addition of thiyl radicals to alkenes (or alkynes), which yield carbon centered radicals (step (ii)), were extensively investigated by Ito et al. in the 1980s using a microsecond flash photolysis method, and have been reviewed previously.[18] Bimolecular reaction rate coefficients for a number of combinations of aromatic thiyl radicals and alkenes or alkynes were deduced by monitoring the kinetics of removal of the thiyl radicals, and the initial addition step was proposed to be reversible.

[a] School of Chemistry, University of Bristol, Cantock's Close, Bristol BS8 1TS, UK
[b] Central Laser Facility, Research Complex at Harwell, Science and Technology Facilities Council, Rutherford Appleton Laboratory, Harwell Oxford, Didcot, Oxfordshire, OX11 0QX, UK
E-mail: A.Orr-Ewing@bristol.ac.uk; Tel: +44 (0)117 9287672

† Electronic Supplementary Information (ESI) available: All experimental data are archived in the University of Bristol's Research Data Storage Facility (DOI 10.5523/bris.6shpaaql5nn1lbf0jotdwc0j). The Supplementary Information contains details of the synthesis of QSSQ, identification of the long-time stable product, TVA spectra of $W(CO)_6$ to characterize the sample flow conditions, TEA and TVA spectra of QSSQ in styrene, TEA spectra of pure MMA, steady state FT-IR spectra of QSSQ, details of fits to a diffusion model, time-dependent shifts for the QS radical band observed in TVA spectra, exponential fittings for observed bands in TVA spectra in $CDCl_3$, examples of spectral decompositions, computed infrared frequencies and potential energy curves for QSSQ, and computed electronic absorption spectra for the QS-St and QS-MMA radical. See DOI: 10.1039/x0xx00000x

The combination of ultrafast transient vibrational absorption spectroscopy (TVAS) and TEAS is powerful for investigation of bimolecular radical-reaction mechanisms because the formation and decay of the initial radical can be monitored by TEAS, with subsequent reaction intermediates observed by TVAS.[19-21] Here, we demonstrate that TVAS at discrete time delays from 200 fs to 50 μs in a single set of measurements, combined with TEAS over a more restricted time range from 100 fs - 1.3 ns, provides a comprehensive view of a sequence of unimolecular initiation and bimolecular addition steps in a radical chain reaction.

We report the continuous observation of a thiol-ene reaction over further steps than were possible in previous TEAS and TVAS measurements of radical reactions.[9, 22, 23] By extending the longest measurement times from the nanosecond to the microsecond range, we capture snapshots of the reaction pathway starting from ultrafast (sub-ps) formation of aromatic thiyl radicals by photodissociation of the corresponding disulfide. Kinetic studies of the steps in a thiol-ene reaction that follow the formation of the carbon centered radical have not been reported previously. Here, we show how such measurements can connect the ultrafast dynamics of initiation of radical reactions to the much longer timescales commonly considered in synthetic chemistry. We chose 1,2-di(quinolin-2-yl)disulfide (denoted as QSSQ) as a thiyl radical source, because the corresponding thiyl radical, quinoliene-2-thiyl (QS) is expected to show fast addition reaction rates with alkenes. This expectation is based on small enthalpies of activation computed for the addition step (ii), as illustrated in Figure 1 for reaction with styrene. High reaction rates of thiol-ene reactions are desirable both in chemical synthesis, and in industrial applications such as light curing of resins or paints, and vulcanization in the rubber industry.

The chemical structures of the QSSQ and QS radical are provided below.

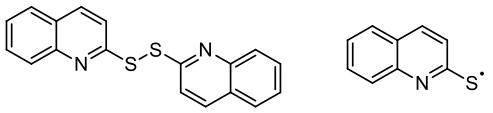

QSSQ QS

The alkene source selected for the reactive studies with QS radical is methyl methacrylate (MMA) because it contains a carbonyl group which is an excellent IR chromophore for TVAS measurements of the reactions that follow formation of the initial carbon centered radical.

2. Experimental Details

1,2-di(quinolin-2-yl)disulfide (QSSQ) was synthesized by a procedure modified from the literature (see Supplementary information for details).[27] Methanol, and deuterated chloroform (99.8 atom % D, Sigma Aldrich) were used as received. Methyl methacrylate (≥ 99%, Sigma Aldrich) was passed through a basic aluminum oxide column prior to use to remove the inhibitor, 4-methoxyphenol.

The transient absorption spectroscopy experiments were performed using the LIFEtime laser system[28, 29] at the Central Laser Facility of the Rutherford Appleton Laboratory (RAL, for temporal windows from 200 fs up to ~50 μs) in continuous measurements, or an ultrafast laser system at the University of Bristol (for temporal windows from 100 fs up to ~1.3 ns). The experimental setups and procedures used for TEAS and TVAS measurements have been described previously,[28-32] therefore only details specific to the present study are provided here.

Measurements were carried out in a Harrick cell with CaF_2 windows separated by a PTFE spacer (380 μm for TEAS and 100 μm for TVAS) and sample solutions were circulated by a peristaltic pump. The photochemistry of QSSQ was initiated by a 330-nm UV pulse (800 nJ/pulse for measurements at the University of Bristol, and 200 nJ/pulse at RAL). This wavelength was chosen to excite one of the main absorption bands of QSSQ: Figure 2 shows the steady state UV/visible absorption spectrum of QSSQ in methanol (MeOH). The QSSQ solutions were prepared to obtain an optical density of ~0.5 OD with the 100 μm or 380 μm spacers at the 330-nm excitation wavelength (1.0 mM for TEAS and 3.8 mM for TVAS experiments). The instrument response function (IRF) was 150 fs for TEAS experiments,[9] ~300 fs for TVAS experiments at the University of Bristol,[32] and < 200 fs for TVAS experiments at RAL.[29] The pure solvents (methanol and MMA) showed transient response signals which contributed backgrounds to the recorded TEA spectra.[9] Therefore, solvent-only spectra were subtracted from the raw TEAS datasets to eliminate contributions from the solvent, as described previously.[9] For TVAS measurements on nanosecond to microsecond time intervals, sample flow out of the probe laser volume perturbed the measured kinetics.[28] Therefore, TVA spectra at each time delay were corrected for flow effects using TVA spectra of tungsten hexacarbonyl ($W(CO)_6$) in cyclohexane solution obtained at the same flow rate as the TVAS measurements of QSSQ.[28] The $W(CO)_6$ data are presented in Figure S1 of Supplementary Information. All measurements were performed without purging molecular oxygen from the sample solutions, unless otherwise specified.

The vertical excitation energies and transition dipole moments (TDMs) of the QS radical were calculated using the Molpro package.[33] The ground state geometry was optimized using Møller-Plesset second-order perturbation theory (MP2) and the aug-cc-pVTZ basis set,[34, 35] using the Gaussian 09 package.[36] The transition dipole moments were then calculated using the state averaged complete active space self-consistent field (SA-CASSCF) method with an aug-cc-pVTZ basis set, and subsequently the vertical excitation energies were corrected using complete active space with second-order perturbation theory (CASPT2) with the SA-CASSCF result as a reference wavefunction. During the calculations, C_s symmetry was adopted, and the SA-CASSCF calculation was carried out by averaging over eight states (four of A' symmetry and four of A" symmetry). An imaginary level shift of 0.3 a.u. was used for all of the CASPT2 calculations to avoid intruder state problems. These calculations included eleven electrons in ten active orbitals (11/10) comprising the sulfur $3p_x$, $3p_y$, the four π and the four corresponding π^* orbitals.

Calculations of harmonic vibrational frequencies, thermodynamic properties and electronic absorption spectra were performed in Gaussian 09. The computations of harmonic vibrational frequencies used the B3LYP density functional,[37, 38] with the 6-311++G(3df,3pd) basis set, and the resulting infrared frequencies were corrected using a linear function obtained by comparison of experimental and computed frequencies for QSSQ, as illustrated in Figures S2 and S3. This procedure gave good agreement between experimental and calculated infrared frequencies for the compounds of interest in this study.[9, 39] Calculations of absorption spectra of the carbon centered addition radical (denoted as QS-MMA for the reaction with MMA) used time-dependent density functional theory (TDDFT) with the 6-311++G(3df,3pd) basis set. Enthalpies of activation for addition reactions of the various aromatic thiyl radical with styrene illustrated in Figure 1 were calculated using the CAM-B3LYP density functional,[40] with the 6-311++G(d,p) basis set, because reliable transition states for the addition reaction could not be obtained with the B3LYP method.[41] The validity of the

transition states was confirmed by subsequent intrinsic reaction coordinate (IRC) calculations.

3. Results and discussion

The photochemical reactions from ultrafast to microsecond timescales initiated by 330-nm UV excitation of QSSQ require a combination of TEAS and TVAS to unravel. The results in non-alkene (non-reactive) solutions are discussed first to obtain fundamental information about the formation and loss of the QS radical in the absence of alkene reaction pathways. We then report results in MMA solution of QSSQ photo-induced reaction kinetics, from the ultrafast formation of QS radicals to diffusive reaction with molecular oxygen. Complementary results for styrene solution are presented in the Supplementary Information, from which we deduce a bimolecular reaction rate coefficient to compare with previously reported values for thiyl radical + styrene reactions.

3.1. Photochemical dynamics of QSSQ in non-alkene solutions

The solvents we chose for study of the short-time photochemical dynamics of QSSQ were MeOH for TEAS and deuterated chloroform ($CDCl_3$) for TVAS. A transient signal from pure MeOH was only seen while the pump and probe laser pulses overlapped in time, in contrast to measurements in MMA, for which TEA spectra are presented in Figure S4. Therefore, precise early time dynamical information can be better obtained in MeOH solution. Our TEAS system covers the probe wavelength region from 330 nm to 625 nm, but transient absorption signals located at wavelengths shorter than 350 nm were masked by the 330-nm excitation pump laser light.

3.1.1. TEAS of QSSQ in methanol solution. Figure 3 shows TEA spectra of 1.0 mM QSSQ in MeOH and the deduced kinetics following 330-nm excitation. In Figure 3(a), there is a prominent band centered at 527 nm, and it shows a slower rise than the IRF of 150 fs,[9] as is demonstrated in the inset to Figure 3(b). A fit with a Gaussian convolution to account for the IRF gives a rise time constant of ~200 fs. We assign it to $\widetilde{B} \leftarrow \widetilde{X}$, and perhaps $\widetilde{C} \leftarrow \widetilde{X}$ absorptions by ground state QS radicals formed by photodissociation of QSSQ because of the observed time constant,[9] and because the band position of 527 nm is in reasonable agreement with the computed excitation wavelengths of these bands with non-zero TDMs presented in Table 1. CASPT2 calculations indicate that the ground and first excited states of the QS radical are energetically close. Hence, we also considered the possibility of absorption bands originating from the photochemically populated $\widetilde{A}$ state, but computed TDMs for possible transitions at wavelengths around 527 nm are negligible (i.e. TDM values are 0.00 for the $\widetilde{B} \leftarrow \widetilde{A}$ transition, and 0.01 for the $\widetilde{C} \leftarrow \widetilde{A}$ transition, see Table 1), and we therefore discounted this possibility. The computed potential energy curves (PECs) for QSSQ provided in Figure S5 also support assignment of absorption features to QS ($\widetilde{X}$): the first singlet excited state of QSSQ is dissociative along the S-S coordinate, and adiabatic correlation through conical intersections leads to $\widetilde{X}$-state QS radicals. The same propensity was found in our previously reported PECs for 2,2'-dithiobis(benzothiazole).[9]

The bands centred at 370 nm and 527 nm show the same time dependence of their decays (within 2 SD uncertainties of fitted time constants), and both are therefore attributed to the QS ($\widetilde{X}$) radical. After reaching their maximum absorptions, the integrated band intensities decay with time constants of $\tau_1 = 3.3 \pm 0.2$ ps and $\tau_2 = 107 \pm 6$ ps for the 370-nm band, and $\tau_1 = 3.5 \pm 0.3$ ps and $\tau_2 = 111 \pm 7$ ps for the 527-nm band if biexponential fitting is employed, and thereafter 36 ± 1% of the initially formed QS radicals survive at the limit of our experimental time delay of ~1.3 ns. The decay behavior is characteristic of recombination of photodissociated aromatic disulfides,[9, 10, 14] and a recombination rate coefficient of $k_{rec} = (3.4 \pm 0.2) \times 10^{10}$ M^{-1} s^{-1} is deduced by adopting the Smoluchowski diffusion model.[42] The calculated rate coefficient also incorporates the formation of a QS radical dimer, as discussed further below. This model was employed by Bultmann et al. for analysis of the cage recombination dynamics of *p*-aminothiophenoxy radicals generated photolytically from bis(*p*-aminophenyl)disulfide,[10] as well as in our previous report on the photochemical reaction dynamics of another aromatic disulfide.[9] The details of our fitting method and interpretation of the biexponential decays are provided in the Supplementary Information and Figure S6.

The early time kinetics shown in the inset to Figure 3(b) differ for the 370-nm and 527-nm bands. In particular, the integrated band intensity of the 370-nm feature reaches its maximum during the IRF whereas the growth of the 527-nm band is slightly delayed. The centre of the 527-nm band shows a small shift to lower wavelength over a few hundred fs which could indicate vibrational cooling of the nascent radicals, dipolar interaction between the caged radical pair, or solvent reorganization. The faster growth of the 370-nm band suggests that absorption from one or more singlet excited states of QSSQ contributes to the 370-nm feature and is dominant over the times of pump-probe laser overlap. There is a hint of a secondary rise in the 370-nm band up to $\Delta t = 1$ ps consistent with a growing contribution from QS($\widetilde{X}$) superimposed on the decay of excited state QSSQ absorption. The same trend at early time delays is evident in the kinetic trace at 432 nm, but careful inspection of Fig. 3(b) over the temporal range up to 20 ps indicates a subtle rise which is not seen for the bands at 370 nm and 532 nm. The time constant for this rise is 10.2 ± 1.1 ps, obtained by single exponential fitting following spectral decomposition with the KOALA program,[43] an example of which is shown in Figure S7. We assigned a similar feature in a prior study to the formation of a π-stacked radical dimer on the basis of the observed timescale and the dependence of absorption intensity on the solvent type.[9, 11, 13] We therefore attribute the growing band centered at 432 nm to a π-stacked QS radical dimer $(QS)_2$ formed through the following reaction scheme:

$$\mathrm{QSSQ} \underset{k_{rev}}{\overset{h\nu}{\rightleftharpoons}} 2\,\mathrm{QS} \xrightarrow[k_{dimer}]{} (\mathrm{QS})_2 \qquad (1)$$

The loss of QS radicals is controlled by both the recombination to QSSQ and to $(QS)_2$, and therefore the deduced rate coefficient of $k_{rec} = (3.4 \pm 0.2) \times 10^{10}$ M^{-1} s^{-1} incorporates both processes.

3.1.2. TVAS of QSSQ in deuterated chloroform solution. Figure 4 shows TVA spectra of 3.8 mM QSSQ in $CDCl_3$ following 330-nm excitation and integrated intensities for the band at 1367 cm^{-1}. All eight negative-going bleach bands at 1091, 1141, 1293, 1421, 1450, 1558, 1586, 1618 cm^{-1} are explained by depletion of the

ground state QSSQ concentration induced by the pump light, as established by comparison with the steady state FTIR spectrum of QSSQ (Figure S2). Positive transient absorptions to the low wavenumber side of the bleach features are in part attributable to production of vibrationally hot, but ground electronic state QSSQ molecules formed by internal conversion from excited electronic states or geminate recombination of QS radical pairs. The parent bleach bands recover with exponential time constants of 24 - 32 ps, as summarized in Table S1, which mostly reflect vibrational cooling rates in solution. Although the time constants for the recovery of all the bleach features are roughly similar, the magnitudes of residual bleaches at long time (reported in Table S1) differ from 15 – 31%. The discrepancy in these values is a consequence of spectral overlaps with the product (positive) bands at 1417, 1550, 1578 and 1606 cm^{-1} seen in the later time spectra in Figure 4(a).

The most easily discernable product band lies at 1367 cm^{-1} and is not overlapped with any parent QSSQ bleach bands. This feature is shown on an expanded scale in Fig. 4(b); it is observed even at our earliest time delay of 0.3 ps for TVAS experiments, and decays on a timescale of ~200 ps, as seen in Figure 4(c), before becoming a persistent feature with almost constant absorption. The decay kinetics fit to a single exponential function with a time constant of 55 ± 3 ps, and 57 ± 1% of the initial intensity remains until 1200 ps. We assign this band to the QS radical formed through photodissociation of QSSQ on the basis of its kinetic behavior and the computed fundamental infrared band positions presented in Table 2. This assignment is further confirmed by the quenching of this band in styrene solution, as discussed in the Supplementary Information. The QS radical band maximum initially locates at 1363 cm^{-1} and shifts to 1367 cm^{-1} with a time constant of ~13 ps (Figure S8). The time constant for the band shift is attributed to vibrational relaxation,[9] although solvent rearrangement or radical pair interaction could contribute. The QS radical is proposed to be initially vibrationally excited because of the energy difference between the first singlet excited state of QSSQ and the ground state of the two product QS radicals, as the potential energy curves in Figure S5 indicate.

The other, less obvious product bands at 1417, 1550, 1578 and 1606 cm^{-1} are also assigned to the QS radical on the basis of their calculated infrared positions and their presence at the earliest time delay of 0.3 ps. However, their kinetic behavior differs somewhat from the band at 1367 cm^{-1}, most likely due to spectral overlaps with the neighboring bleach bands, as shown in Table S1. For example, the bands at 1548 cm^{-1} and 1575 cm^{-1} almost completely decay with respective time constants of 28 ± 1 ps and 26 ± 1 ps, which match the bleach recovery time constants associated with cooling of hot ground-state molecules. Hence, the interpretation of product bands, with the exception of the band at 1367 cm^{-1}, should be treated with caution. The largest long-time residual amplitude for the QSSQ bleach band at 1293 cm^{-1} is 31%, and the data plotted in Fig. 4(c) indicate that 57% of the QS + QS pairs formed by QSSQ photolysis diffuse apart, whereas 43% recombine to QSSQ or $(QS)_2$. Consequently, we estimate the quantum yield for initial formation of caged QS radical pairs from the photodissociation of QSSQ to be ~54%.

3.2. Photo-induced reactions of QSSQ in methyl methacrylate solution

In this section, we discuss the photochemical reaction of QS radicals with MMA from initiation by photodissociation of QSSQ until completion of the reactions of the carbon-centered radicals resulting from QS + MMA addition. These observations of sequential steps in the radical reaction scheme require picosecond to microsecond TVAS measurements. First, we report TEAS results obtained in neat MMA to confirm an addition reaction. Then, we concentrate on TVAS results obtained for aerated and N_2-purged solutions. For the TVAS experiments, strong absorptions prevented us from using neat MMA, and therefore we diluted the MMA by a factor of 100 (i.e., samples were 3.8 mM QSSQ / 100 mM MMA in $CDCl_3$ solution). Table 3 summarizes the rate coefficients derived from TVAS measurements reported in this section.

Figure 5 shows TEA spectra of 1.0 mM QSSQ in neat MMA solution. The QS bands, one of which has an absorption peak at 525 nm, decay almost completely, in contrast to the MeOH solution measurements discussed in Section 3.1.1. The complete removal of the QS radical signatures is indicative of reaction with MMA,[9] in addition to recombination and $(QS)_2$ dimer formation on similar timescales (see Section 3.1.1). The growth kinetics for the reaction product can also be estimated from the TEA spectra because a broad product band centered at around 425 nm is evident at later time delays. This band extends as far as the longer wavelength edge of our probe window (625 nm). Spectral decomposition with the KOALA program,[43] indicates an approximately nanosecond timescale growth. We assign this broad feature in the TEA spectra to the carbon centered radical (denoted as QS-MMA) formed from the following addition reaction of QS with MMA, on the basis of the computed electronic absorption spectrum for QS-MMA plotted in Figure S9:

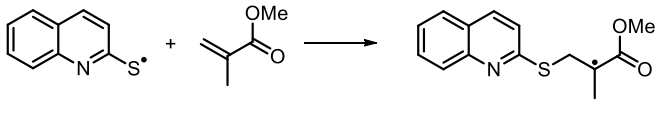

(2)

The above assignment is further confirmed by TVAS results discussed below.

We fitted the two data sets in Figure 5(b) using a combination of the Smoluchowski diffusion model (eq. (1) in Supporting Information) and a single exponential function to describe loss of QS and growth of QS-MMA from reaction of QS with MMA. This fit gave an exponential time constant τ_1 = 1120 ± 150 ps.

Figure 6 shows TVA spectra of 3.8 mM QSSQ / 100 mM MMA in aerated $CDCl_3$ solution and compares the time-dependence of the integrated band intensities (panels (b) and (c)) with those obtained for solutions purged of dissolved oxygen by N_2 bubbling (panels (d) and (e)). The corresponding TVA spectra of QSSQ in $CDCl_3$ and in 100 mM MMA in N_2-bubbled $CDCl_3$ solution are provided in Figure S11 and S12. Before a time delay of ~1 ns, we did not see any obvious product features in these reaction systems, except for the QS radical bands

discussed in Section 3.1.2. The negative bands at 1091, 1141, 1421, 1450, 1496, 1558, 1586 and 1618 cm^{-1} are attributed to QSSQ bleaches. The negative-going bands at 1168 cm^{-1} and around 1700 cm^{-1} correspond to MMA features, an assignment confirmed by comparison with a steady state FTIR spectrum of MMA. In addition, five product bands at 1088, 1102, 1137, 1595 and 1653 cm^{-1} (3 of which are marked by arrows in Fig. 6(a)), not seen for QSSQ in $CDCl_3$ (Figure S11), become evident at time delays approaching ~1 μs.

The representative product bands at 1088 and 1595 cm^{-1} grow with respective time constants of 102 ± 13 ns and 98 ± 8 ns obtained by spectral decomposition (see Figure S13), and show almost constant absorbance after their growth. The product band at 1653 cm^{-1} evolves with a similar time constant to the two bands at 1088 and 1595 cm^{-1}, but this band decays after reaching its maximum intensity at a time delay of 300 ns. We focus on this characteristic kinetic trace later in this section.

For three reasons, we assign the growing product bands to QS-MMA formed by the addition of a QS radical to MMA, as is illustrated in reaction scheme (2). The first reason is that the observed infrared positions are in excellent agreement with the computed infrared frequencies for the QS-MMA radical presented in Table 4. The observed band at 1653 cm^{-1} is the most evident signature for the formation of QS-MMA: on the basis of our DFT calculations, this band corresponds to the C=O stretch mode of the MMA moiety in the QS-MMA radical. It appears at the lower wavenumber side of the corresponding C=O stretch mode of the parent MMA, which has an absorption centered at 1719 cm^{-1}. The shift of the carbonyl band position of the QS-MMA radical to lower wavenumber is a result of an elongation of the bond caused by conjugation with the radical at the α-carbon site (1.218 Å for the QS-MMA radical and 1.207 Å for MMA, according to our DFT calculations). The second reason is the qualitative consistency of the deduced time constants for the product bands with a time constant for development of the MMA bleach band at 1168 cm^{-1} of 294 ± 36 ns. This time constant is approximately three times larger than the ~100 ns growth of the product bands at 1088 and 1595 cm^{-1}. The discrepancy is a consequence of underlying product bands from a subsequent reaction with dissolved O_2. The third piece of evidence is the timescale for the formation of QS-MMA radicals: considering the dilution factor of 100 for this TVAS experiment, the timescale of a few hundred nanoseconds for the reaction is consistent with the ~ nanosecond formation of QS-MMA in neat MMA solution estimated from our TEAS measurements.

After reaching their maximum intensities at time delays of ~300 ns, the integrated intensities for the bands at 1088 cm^{-1} and 1595 cm^{-1} remain almost constant, whereas the band at 1653 cm^{-1}, the C=O stretch mode of the QS-MMA radical, decays over our full temporal window of ~50 μs. This kinetic behavior can be understood if the QS-MMA radical is involved in further reactions which remove the carbon radical at the α-position, and new products have bands at 1088 cm^{-1} and 1595 cm^{-1} with comparable infrared absorption cross-sections to those of the QS-MMA radical. One candidate product which meets these criteria is a peroxy radical species, denoted by QS-MMA-O_2. It has computed bands at 1085 and 1594 cm^{-1} with intensities similar to those of QS-MMS (see Table 4), but a carbonyl stretch which shifts to higher wavenumber by more than 100 cm^{-1}.

Reactions of carbon centered radicals with molecular oxygen are well known,[18, 44] and are a likely source of QS-MMA-O_2. We therefore compared the TVAS data with measurements under oxygen-purged conditions, which eliminate the possibility of QS-MMA-O_2 formation. The time-dependences of the bands at 1595 cm^{-1} and 1653 cm^{-1} are shown in Figure 6(d) for the nanosecond regime and (e) for the microsecond regime. The band at 1595 cm^{-1} grows with a time constants of 94 ± 15 ns in the purged solution, indicating no obvious effect from molecular oxygen on the formation of QS-MMA.

When we concentrate on the kinetic behavior on the microsecond timescale, after the formation of QS-MMA (Figure 6(c) and (e)), the influence of molecular oxygen on the kinetic traces for the band at 1653 cm^{-1} is apparent. A single exponential function adequately fits the decay kinetics at 1653 cm^{-1} obtained in the N_2-bubbled solution, giving a time constant of 42 ± 16 μs, whereas in the aerated solution, an additional fast decay component is confirmed for the decay of the QS-MMA C=O stretch mode, and a biexponential function is required to fit the decay, giving $\tau_1 = 0.58 \pm 0.07$ μs and $\tau_2 = 52 \pm 19$ μs. The faster decay component observed in the aerated solution indicates reaction of QS-MMA with molecular oxygen:

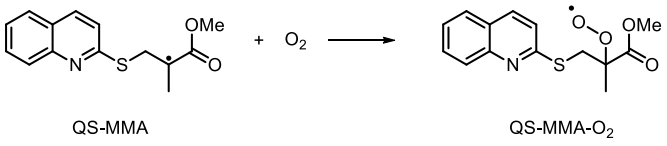

(3)

Although formation of peroxy radicals from reactions of carbon centered radicals with dissolved molecular oxygen has been proposed previously by monitoring loss of thiyl radicals,[18, 44] our observation is more direct because we measure the decay of the carbon centered radical. The calculated infrared band intensities and positions for QS-MMA-O_2 provided in Table 4 support our interpretation. Moreover, we identify that the main final product under our photochemical reaction conditions (i.e. in the presence of molecular oxygen) is the hydroxysulfide QS-MMA-OH, for which the chemical structure is presented below (see the Supplementary Information for details of this product characterization). We also detect at least two minor side products with unidentified chemical structures.

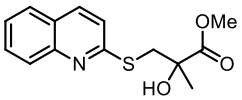

QS-MMA-OH

The formation of hydroxysulfides from addition reactions of thiyl radicals with alkenes in the presence of molecular oxygen has been reported previously,[45-47] and therefore the above assignment of the fast decay component to the production of QS-MMA-O_2 in the aerated solution is further supported.

The decay of the band at 1653 cm^{-1} is comprised of at least two components, as seen in Figure 6(c) and discussed earlier. We estimate the concentration of the QS-MMA radical in the probed sample volume to be 0.30 mM under our experimental conditions, using a pump energy of 200 nJ/pulse, pump beam diameter of 100 μm,[28, 31] sample pathlength of 100 μm, optical density of QSSQ of 0.5 OD, and a quantum yield for the survival of the two QS radicals of 31% (Table S1). The concentration of molecular oxygen in aerated $CDCl_3$ solution is 2.4 mM assuming the solubility of molecular oxygen in $CDCl_3$ is the same as $CHCl_3$.[48] Hence, the concentration of molecular oxygen is in excess over QS-MMA, suggesting that the QS-MMA should be completely consumed by reaction (3). However, only 51 ± 3% of the loss of QS-MMA band intensity is attributed to the faster reactive component corresponding to this reaction with O_2. This kinetic behavior can be understood if reaction (3) is a reversible process. Our DFT calculations at the B3LYP/6-311++G(3df,3pd) level of theory indicate that the Gibbs free energy change for reaction (3) is only moderately negative (-4.8 kJ/mol), which supports this proposal.

The following sequential kinetic model summarizes the reaction of QS radical with MMA in the aerated solution:

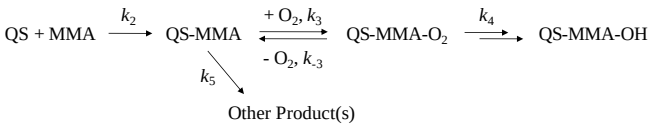

(4)

In the above model, k_5 represents the slow decay component observed in both the N_2-bubbled and aerated solutions. This slow component could correspond to the formation of two undefined minor side products as mentioned earlier, and to dimer formation and H(D)-atom abstraction reactions (reactions (iii) and (vi) described in the Introductory section); the almost constant absorbance after ~1 μs for the MMA bleach band at 1168 cm^{-1} (Figure 6(c)) discounts possible propagation reactions (reaction (vii) in the Introduction). The reasonable agreement of the deduced time constant for the slower component (52 ± 19 μs) with the time constant of 42 ± 16 μs obtained in the N_2 bubbled solution supports these arguments, because the dimerization and H(D)-atom abstraction reaction are possible even under O_2-free conditions.

The fitting of the time-dependence of the band intensity at 1653 cm^{-1} in the aerated $CDCl_3$ solution to the sequential kinetic model (4) assumed a value for the ratio k_3/k_{-3} = 7.17 which we estimated from the computed Gibbs free energy change of -4.8 kJ/mol for the reaction producing QS-MMA-O_2. We also approximated $k_4 + k_5 = k_6$ (i.e. a single, first-order rate coefficient) to fit the long-time decay component. The fitting reproduces the observed time-dependence well, as seen in Figures 6(b) and (c), and gives $k_2' = (2.8 \pm 0.2) \times 10^6$ s^{-1}, $k_3' = (7.9 \pm 0.7) \times 10^6$ s^{-1}, $k_6 = (2.0 \pm 0.2) \times 10^4$ s^{-1}, with pseudo first-order rate coefficients $k_2' = k_2$ [MMA] and $k_3' = k_3$ [O_2]. A similar fitting that excludes the reversible O_2 addition process (k_{-3}) was unsuccessful.

Accordingly, bimolecular reaction rate coefficients are deduced of $k_2 = (2.8 \pm 0.2) \times 10^7$ M^{-1} s^{-1} for the reaction of QS with MMA at a concentration of 100 mM, and $k_3 = (3.3 \pm 0.3) \times 10^9$ M^{-1} s^{-1} for the reaction of QS-MMA with molecular oxygen (assuming [O_2] = 2.4 mM). The former rate coefficient agrees satisfactorily with a value of $(3.4 \pm 0.4) \times 10^7$ M^{-1} s^{-1} estimated by using the time constant for growth of the MMA bleach feature at 1168 cm^{-1}. The deduced reaction rate coefficient for the addition reaction of QS with MMA is ~50 times slower than that with styrene (see the Supplementary Information). This difference can be rationalized by considering the activation barriers for the addition reactions: our DFT calculations at the CAM-B3LYP/6-311++G(d,p) level of theory predict that the enthalpy of activation for the reaction of QS with MMA is 7.2 kJ/mol, whereas that with styrene is 0.8 kJ/mol as illustrated in Figure 1.

Conclusions

The 330-nm UV photo-induced reactions of QSSQ have been studied by a combination of transient electronic and vibrational absorption spectroscopy. The production of QS radicals, the initial addition step in a thiol-ene reaction, and the subsequent reaction of the resulting carbon centered radical with molecular oxygen have been observed by TVAS in a continuous sequence of measurements at discrete time intervals from 200 fs – 50 μs.

Following the 330-nm excitation, the ground state QS radical forms with a time constant of ~200 fs and shows a prominent absorption band centered at 527 nm in methanol solution. The QS radical concentration decays with a rate coefficient of (3.4 ± 0.2) × 10^{10} M^{-1} s^{-1} in methanol solution, because of recombination and formation of a QS radical dimer, but (36 ± 1)% of the initially formed pairs of QS radical persist as separated radicals until the limit of our probe window for TEAS (~1.3 ns). TVAS measurements in deuterated chloroform solution detect a QS radical band at 1367 cm^{-1}, and suggest that the nascent QS radical is vibrationally excited and relaxes to the ground vibrational level with a time constant of ~13 ps.

When methyl methacrylate (MMA) is used as an alkene source, the carbon centered radical QS-MMA forms through addition of QS to MMA, and a bimolecular reaction rate coefficient of (2.8 ± 0.2) × 10^7 M^{-1} s^{-1} is deduced. Infrared absorption bands at 1088, 1102, 1137, 1595, 1653 cm^{-1} are attributed to the QS-MMA radical in $CDCl_3$ solution. The band at 1653 cm^{-1} is free from spectral overlap, and is assigned to the C=O stretch mode.

In solutions purged of dissolved O_2, the 1653 cm^{-1} band of QS-MMA decays gradually over the probe window (~50 μs), suggesting the QS-MMA radical is involved in further reactions on this timescale. These reactions could correspond to dimerization or H(D)-atom abstraction. In contrast, in aerated solutions the more rapid decay of the band intensity at 1653 cm^{-1} with a time constant of 0.58 ± 0.07 μs is attributed to the reaction of QS-MMA with dissolved molecular oxygen, yielding the QS-MMA-O_2 peroxy radical. A bimolecular reaction rate coefficient of (3.3 ± 0.3) × 10^9 M^{-1} s^{-1} is estimated for this reaction. This reaction step is proposed to be reversible on the basis of

incomplete decay of the band at 1653 cm^{-1} and kinetic fitting. The QS-MMA-O_2 radical converts to the stable final product QS-MMA-OH. This study demonstrates that transient absorption spectroscopy can observe chemical processes in continual measurements from the ultrafast (sub-femtosecond) timescale of photochemical initiation to the microsecond or longer timescales more commonly explored in mechanistic organic chemistry.

Acknowledgements

We thank the European Research Council (ERC, Advanced Grant 290966 CAPRI) for financial support. The LIFEtime instrument at the Central Laser Facility is supported by the Biotechnology and Biological Sciences Research Council (BBSRC grant BB/L014335/1) and the Science and Technology Facilities Council. The authors thank Dr. Gregory M. Greetham, Dr. Ian P. Clark, Hugo J. B. Marroux and Dr. Katharina Röttger for their assistance in collecting the experimental data presented in this paper, and Dr. Daniel Murdock for advice on the electronic structure calculations.

References

1. T. Posner, *Ber. Dtsch. Chem. Ges.*, 1905, **38**, 646-657.
2. H. C. Kolb, M. G. Finn and K. B. Sharpless, *Angew. Chem. Int. Ed.*, 2001, **40**, 2004-2021.
3. B. M. Trost, *Science*, 1991, **254**, 1471-1477.
4. B. M. Trost, *Angew. Chem. Int. Ed. Engl.*, 1995, **34**, 259-281.
5. C. E. Hoyle and C. N. Bowman, *Angew. Chem. Int. Ed.*, 2010, **49**, 1540-1573.
6. F. Dénès, M. Pichowicz, G. Povie and P. Renaud, *Chem. Rev.*, 2014, **114**, 2587-2693.
7. S. P. S. Koo, M. M. Stamenović, R. A. Prasath, A. J. Inglis, F. E. D. Prez, C. Barner-Kowollik, W. V. Camp and T. Junkers, *J. Polym. Sci. A Polym. Chem.*, 2010, **48**, 1699-1713.
8. T. A. A. Oliver, Y. Zhang, M. N. R. Ashfold and S. E. Bradforth, *Faraday Discuss.* , 2011, **150**, 439-458.
9. D. Koyama and A. J. Orr-Ewing, *Phys. Chem. Chem. Phys.*, 2016, **18**, 12115-12127.
10. T. Bultmann and N. P. Ernsting, *J. Phys. Chem.*, 1996, **100**, 19417-19424.
11. Y. Hirata, Y. Niga, S. Makita and T. Okada, *J. Phys. Chem. A*, 1997, **101**, 561-565.
12. Y. Hirata, Y. Niga, M. Ohta, M. Takizawa and T. Okada, *Res. Chem. Intermed.*, 1995, **21**, 823-836.
13. A. Lochschmidt, N. Eilers-Konig, N. Heineking and N. P. Ernsting, *J. Phys. Chem. A*, 1999, **114**, 2587-2693.
14. T. W. Scott and S. N. Liu, *J. Phys. Chem.*, 1989, **93**, 1393-1396.
15. T. A. A. Oliver, G. A. King, D. P. Tew, R. N. Dixon and M. N. R. Ashfold, *J. Phys. Chem. A*, 2012, **116**, 12444-12459.
16. Y. Zhang, T. A. A. Oliver, S. Das, A. Roy, M. N. R. Ashfold and S. E. Bradforth, *J. Phys. Chem. A*, 2013, **117**, 12125-12137.
17. Y. Zhang, T. A. A. Oliver, M. N. R. Ashfold and S. E. Bradforth, *Faraday Discuss.*, 2012, **157**, 141-163.
18. O. Ito, *Res. Chem. Intermed.*, 1995, **21**, 69-93.
19. M. S. Platz, *J. Org. Chem.*, 2014, **79**, 2341-2353.
20. A. C. Crowther, S. L. Carrier, T. J. Preston and F. F. Crim, *J. Phys. Chem. A*, 2008, **112**, 12081-12089.
21. A. J. Orr-Ewing, *Annu. Rev. Phys. Chem.*, 2015, **66**, 119-141.
22. D. Koyama, P. Coulter, M. P. Grubb and A. J. Orr-Ewing, *J. Phys. Chem. A*, 2015, **119**, 12924-12934.
23. P. C. Coulter, M. P. Grubb, D. Koyama and A. J. Orr-Ewing, *J. Phys. Chem. A*, 2015, **119**, 12911-12923.
24. O. Ito, K. Nogami and M. Matsuda, *J. Phys. Chem.*, 1981, **85**, 1365-1368.
25. O. Ito and M. Matsuda, *J. Am. Chem. Soc.*, 1979, **101**, 5732-5735.
26. O. Ito and M. Matsuda, *J. Org. Chem.*, 1983, **48**, 2410-2412.
27. B. Zeynizadeh, *J. Chem. Res. (S)*, 2002, 564-566.
28. G. M. Greetham, D. Sole, I. P. Clark, A. W. Parker, M. R. Pollard and M. Towrie, *Rev. Sci. Instrum.*, 2012, **83**, 103107.
29. G. M. Greetham, P. M. Donaldson, C. Nation, I. V. Sazanovich, I. P. Clark, D. J. Shaw, A. W. Parker and M. Towrie, *Appl. Spectrosc.*, 2016, **70**, 645-653.
30. G. M. Roberts, H. J. B. Marroux, M. P. Grubb, M. N. R. Ashfold and A. J. Orr-Ewing, *J. Phys. Chem. A*, 2014, **118**, 11211-11225.
31. G. M. Greetham, P. Burgos, Q. Cao, I. P. Clark, P. S. Codd, R. C. Farrow, M. W. George, M. Kogimtzis, P. Matousek, A. W. Parker, M. R. Pollard, D. A. Robinson, Z. Xin and M. Towrie, *Appl. Spectrosc.*, 2010, **64**, 1311-1319.
32. K. Röttger, H. J. B. Marroux, H. Böhnke, D. T. J. Morris, A. T. Voice, F. Temps, G. M. Roberts and A. J. Orr-Ewing, *Faraday Discussions*, 2016, **194**, 683-708.
33. H.-J. Werner, P. J. Knowles, G. Knizia, F. R. Manby, M. Schütz, P. Celani, T. Korona, R. Lindh, A. Mitrushenkov, G. Rauhut et al. *MOLPRO, version 2010.1, A Package of Ab Initio Programs* 2010.
34. T. H. J. Dunning, *J. Chem. Phys.*, 1989, **90**, 1007-1023.
35. D. E. Woon and T. H. J. Dunning, *J. Chem. Phys.*, 1993, **98**, 1358-1371.
36. M. J. Frisch, G. W. Trucks, H. B. Schlegel, G. E. Scuseria, M. A. Robb, J. R. Cheeseman, G. Scalmani, V. Barone, B. Mennucci, G. A. Petersson et al. *Gaussian 09, Gaussian Inc., Wallingford CT*, 2009.
37. C. Lee, W. Yang and R. G. Parr, *Phys. Rev. B*, 1988, **37**, 785-789.
38. A. D. Becke, *J. Chem. Phys.*, 1993, **98**, 5648-5652.
39. D. Koyama and A. J. Orr-Ewing, *Phys. Chem. Chem. Phys.*, 2016, **18**, 26224-26235.
40. T. Yanai, D. P. Tew and N. C. Handy, *Chemical Physics Letters*, 2004, **393**, 51-57.
41. N. Chéron, D. Jacquemin and P. Fleurat-Lessard, *Phys. Chem. Chem. Phys.*, 2012, **14**, 7170-7175.
42. S. A. Rice, *Diffusion-Limited Reactions, Elsevier, Amsterdam*, 1985.
43. M. P. Grubb, A. J. Orr-Ewing and M. N. R. Ashfold, *Rev. Sci. Instrum*, 2014, **84**, 064104.
44. X. Zhang, N. Zhang, H. Schuchmann and C. Sonntag, *J. Phys. Chem.*, 1994, **98**, 6541-6547.
45. H. Xi, B. Deng, Z. Zong, S. Lu and Z. Li, *Org. Lett.*, 2015, **17**, 1180-1183.
46. C. Huo, Y. Wang, Y. Yuan, F. Chen and J. Tang, *Chem. Commun.*, 2016, **52**, 7233-7236.
47. M. Ueda, H. Miyabe, H. Shimizu, H. Sugino, O. Miyata and T. Naito, *Angew. Chem. Int. Ed.*, 2008, **47**, 5600-5604.
48. *Handbook of Photochemistry, 3rd Edn. CRC Press, Boca Raton 2006*.

Figure1

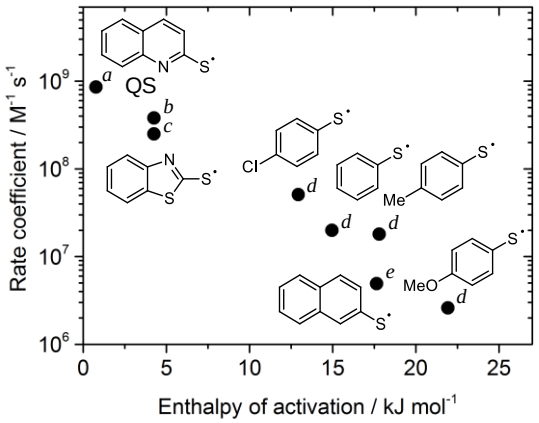

Figure 1: Rate coefficients for the addition reactions of thiyl radicals with styrene and computed enthalpies of activation, obtained at the CAM-B3LYP/6-311++(d,p) level of theory. [a] predicted value from the calculated enthalpy of activation for reaction of QS radical and styrene, and the other seven rate coefficients in the figure. Reported rate coefficients are from: [b] reference [9]; [c] reference [24]; [d] reference [25]; [e] reference [26].

Figure 2

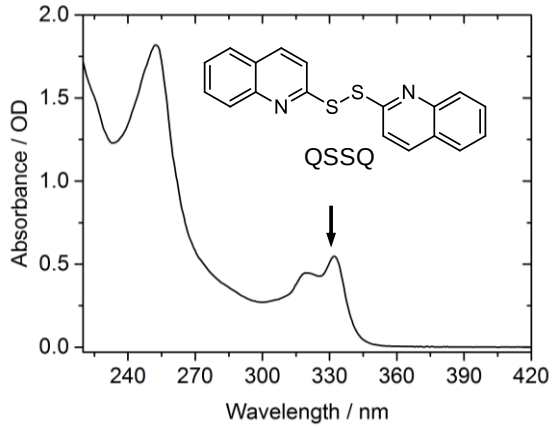

Figure 2: Steady state UV/vis absorption spectrum of 1.0 mM QSSQ in methanol. The spectrum was taken using a 380 μm pathlength sample. The arrow in the figure indicates the excitation wavelength (330 nm) used in this study.

Journal Name

ARTICLE

Figure 3

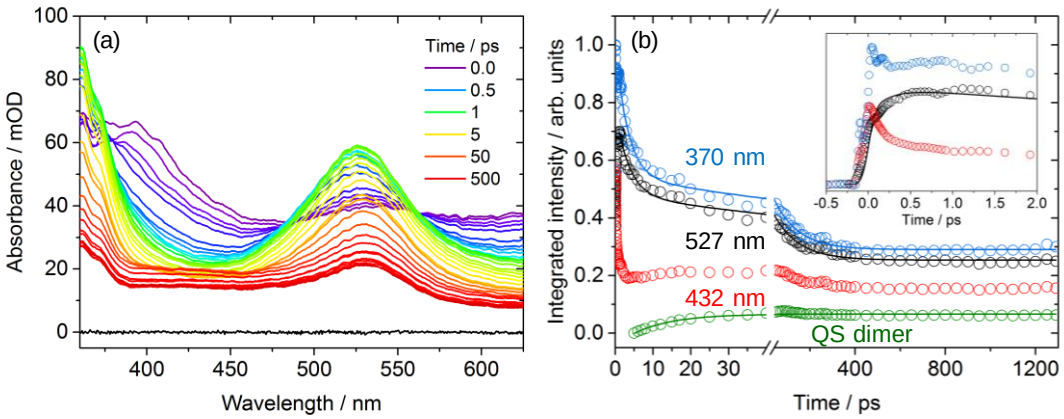

Figure 3: Production of QS radicals from QSSQ photolysis in methanol. (a) Transient electronic absorption spectra of 1.0 mM QSSQ in MeOH following 330-nm excitation. A spectrum at negative time delay is provided in black as a baseline. (b) Integrated intensities for the bands at 370 nm (blue), 432 nm (red) and 527 nm (black), and for the QS radical dimer band (green) obtained by spectral decomposition (see main text). The decomposition was carried out using the TEA spectrum at 5 ps as a basis function for the spectrum of the QS radical and a Gaussian function for the QS radical dimer absorption band. This method assumes that spectral band shapes do not change with time. The solid lines represent biexponential fitting of the intensities for the bands at 370 nm and 527 nm, and a single exponential fitting for the QS radical dimer band, which was obtained by omitting the first 5 ps. Inset: time-dependence at 370 nm, 432 nm and 527 nm for the first 2.0 ps, and a Gaussian convoluted rise and decay using the IRF of 150 fs for the band at 527 nm (solid line).

Table 1: Computed Excitation Energies and Transition Dipole Moments for the QS Radical, Obtained at the CASPT2(11/10)/aug-cc-pVTZ and CASSCF(11/10)/aug-cc-pVTZ Levels of Theory.

Transition	Excitation energy / eV	Excitation wavelength / nm	Transition dipole moment / Debye
$\widetilde{A} \leftarrow \widetilde{X}$	0.08		0.02
$\widetilde{B} \leftarrow \widetilde{X}$	2.44	508	1.35
$\widetilde{C} \leftarrow \widetilde{X}$	2.73	454	1.09
$\widetilde{D} \leftarrow \widetilde{X}$	3.21	386	0.00
$\widetilde{E} \leftarrow \widetilde{X}$	3.40	365	0.56
$\widetilde{B} \leftarrow \widetilde{A}$	2.36	525	0.00
$\widetilde{C} \leftarrow \widetilde{A}$	2.65	467	0.01
$\widetilde{D} \leftarrow \widetilde{A}$	3.13	395	0.04
$\widetilde{E} \leftarrow \widetilde{A}$	3.32	373	0.00

Figure 4

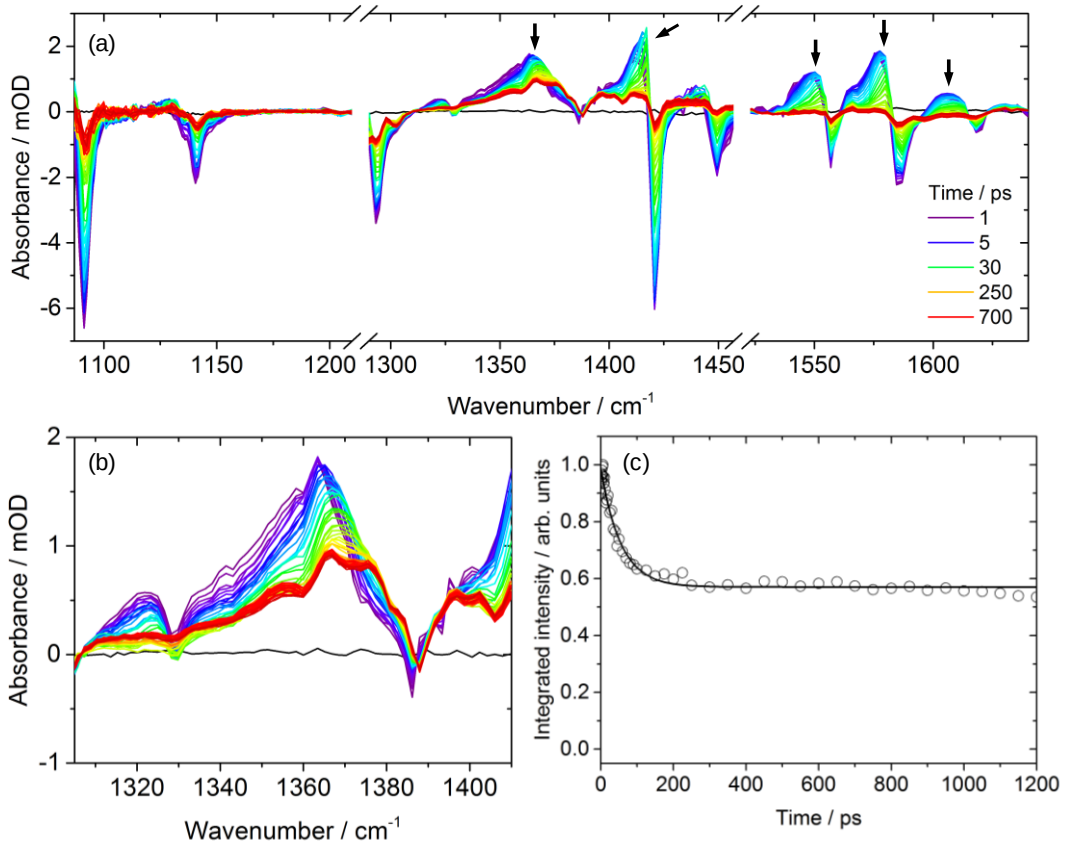

Figure 4: Photolysis and recovery of QSSQ in $CDCl_3$ solution. (a) Transient vibrational absorption spectra of 3.8 mM QSSQ in $CDCl_3$ solution following 330-nm excitation. A spectrum at negative time delay (black) provides a baseline. The arrows in the figure identify the infrared positions of the product bands mentioned in the main text. (b) Expanded view of TVA spectra for the infrared region from 1305 cm^{-1} – 1410 cm^{-1} (with the same colour scheme as panel (a)). (c) Time-dependent integrated band intensity for the band at 1367 cm^{-1}.

Table 2: Computed Fundamental Infrared Transition Frequencies and Intensities, and Observed Infrared Frequencies for the QS Radical.

Calculation [a]		Experiment
Frequency [b] / cm^{-1}	Intensity [c] / km mol^{-1}	Frequency / cm^{-1}
1084	103	-[d]
1140	50	-[d]
1290	37	-[d]
1359	21	1367
1419	36	1417[e]
1497	34	-[d]
1551	55	1550[e]
1590	117	1578[e]
1614	38	1606[e]

[a] Calculations used the Gaussian 09 package and the B3LYP functional with the 6-311++G(3df,3pd) basis set.
[b] Calculated infrared frequencies over our experimental probe region (1080 cm^{-1} – 1670 cm^{-1}). The infrared positions presented in the table are corrected by a linear function obtained by comparing the experimental and calculated frequencies for QSSQ (Figure S3).
[c] Only calculated bands with band intensities greater than 20 km mol^{-1} are shown.
[d] Not observed or uncertain due to spectral overlap with the QSSQ bleach band.
[e] Partially overlapped with the QSSQ bleach band.

Figure 5

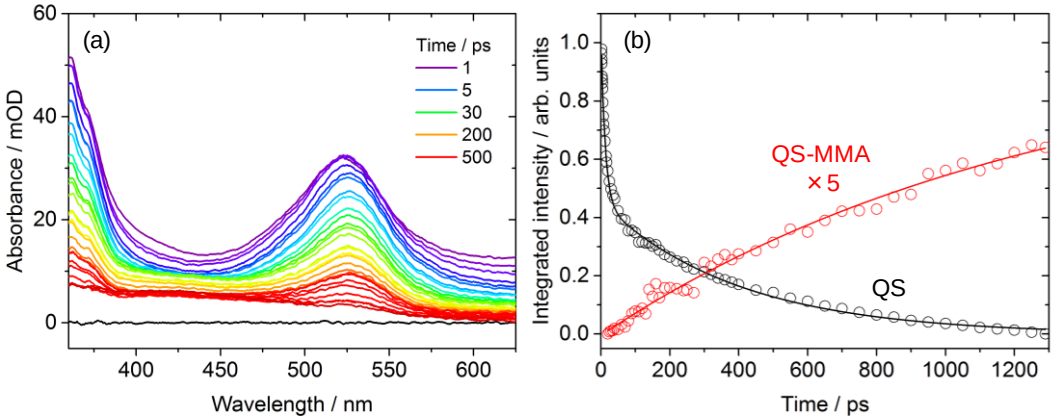

Figure 5: Formation and loss of QS radicals and growth of reaction products in MMA solution. (a) Transient electronic absorption spectra of 1.0 mM QSSQ in MMA following 330-nm excitation. A spectrum at negative time delay shown in black provides a baseline. (b) Integrated band intensities for the QS radical band (black), and QS-MMA band (red) obtained by spectral decomposition with the KOALA program.[43] The integrated intensity for the QS-MMA radical has been multiplied by a factor of 5 for clarity. The decomposition was carried out using the TEA spectrum at 10 ps as representative of the QS radical band, and the spectrum at 1300 ps for the QS-MMA radical band. An example of the decomposition is provided in Figure S10. The solid lines show a fit to the QS radical and QS-MMA bands using a method described in the main text.

Figure 6

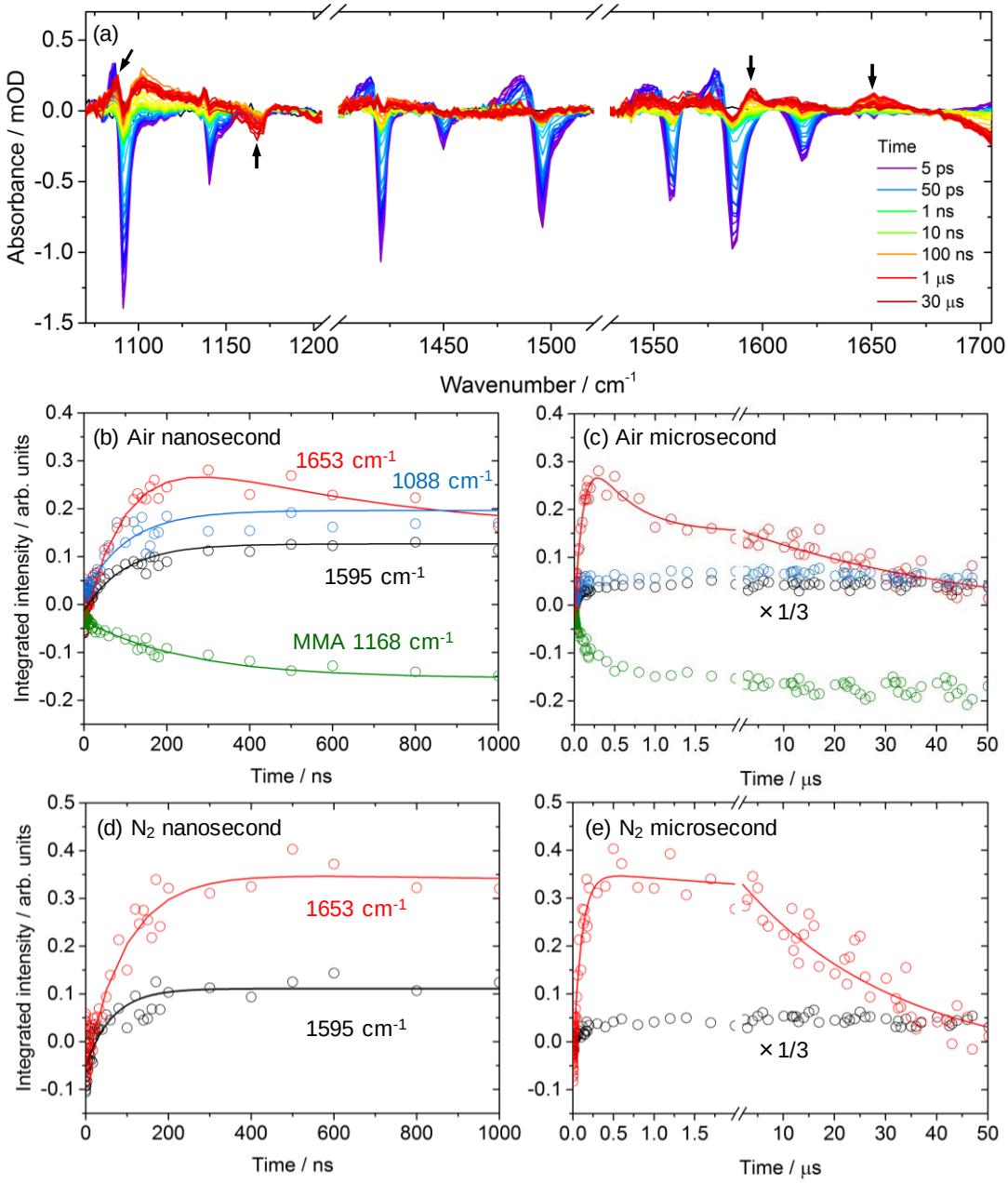

Figure 6: Production and reaction of QS radicals in MMA solutions observed by TVAS. (a) Transient vibrational absorption spectra of 3.8 mM QSSQ / 100 mM MMA in aerated $CDCl_3$ solution following 330-nm excitation. The arrows correspond to the band positions indicated in panels (b) and (c). (b) – (e) Time-dependence of the integrated band intensity at 1088 cm^{-1} (blue), 1168 cm^{-1} (green), 1595 cm^{-1} (black) and 1653 cm^{-1} (red) in the aerated solution ((b) and (c)), and in N_2 bubbled solution ((d) and (e)). The band intensities for the bands at 1088 cm^{-1} and 1595 cm^{-1} in panel (c) and (e) are divided by a factor of three for clarity of representation of the fit to intensities of the band at 1653 cm^{-1}. The kinetic traces for the bands at 1088 cm^{-1} and 1595 cm^{-1} were obtained by spectral decomposition with the KOALA program, using the TVA spectrum at 10 ps as a basis function for the QSSQ bleach. At this time delay, vibrational relaxation of either neighboring QS radical or QSSQ band is almost complete. An example of the decomposition is illustrated in Figure S11. The solid lines for the intensities of bands at 1088, 1168 and 1595 cm^{-1} are single exponential fits, obtained for time delays of 100 ps to 2000 ns, and the line for the band at 1653 cm^{-1} corresponds to a fit to the sequential kinetic model (4). The fitting of the band intensity at 1653 cm^{-1} for the N_2 bubbled solution gives $k_2' = (3.3 \pm 0.2) \times 10^6\ s^{-1}$, $k_5 = (3.0 \pm 0.2) \times 10^4\ s^{-1}$. The corresponding TVA spectra of QSSQ in the N_2 bubbled solution are provided in Figure S12.

Table 3: Summary of First and Second Order Rate Coefficients Obtained by TVAS of QSSQ / 100 mM MMA in $CDCl_3$ Solutions.

	QS + MMA		QS-MMA + O_2		QS-MMA (slow reaction component)	
Band position / cm^{-1}	k / μs^{-1}	k_2 / M^{-1} s^{-1}	k / μs^{-1}	k_3 / M^{-1} s^{-1}	k / μs^{-1}	k_6 / μs^{-1}
1088	9.8 ± 1.3	-	-	-	-	-
1595	10.2 ± 1.0	-	-	-	-	-
1653	-	(2.8 ± 0.2) × 10^7	1.7 ± 0.2	(3.3 ± 0.3) × 10^9	0.019 ± 0.003	0.020 ± 0.002
1168 (MMA bleach)	3.4 ± 0.4		-	-	-	-
1653 (N_2 purged)	-	(3.3 ± 0.2) × 10^7	-	-	0.024 ± 0.009	0.030 ± 0.002

Table 4: Calculated Fundamental Infrared Frequencies and Intensities, and Observed Infrared Band Positions for the QS-MMA and QS-MMA-O_2 Radicals.

Calculation [a]				Experiment
QS-MMA		QS-MMA-O_2		
Frequency [b] / cm^{-1}	Intensity [c] / km mol^{-1}	Frequency [b] / cm^{-1}	Intensity [c] / km mol^{-1}	Frequency / cm^{-1}
1084	115	1085	89	1088
1106	176	1096	74	1102
1137	83	1138	62	1137
1176	214	1180	71	-[d]
1550	61	1552	50	-[d]
1594	143	1594	135	1595
1646	198	1751[e]	197	1653

[a] Calculations used the Gaussian 09 package and the B3LYP functional with the 6-311++G(3df,3pd) basis set.
[b] Calculated infrared frequencies over our experimental probe region (1070 cm^{-1} – 1200 cm^{-1} and 1410 cm^{-1} – 1700 cm^{-1}).
[c] Only calculated bands with band intensities greater than 50 km mol^{-1} are shown.
[d] Not observed due to spectral overlap with QSSQ or MMA bleach bands.
[e] Out of our probe window, but shown for comparison with the infrared position of the C=O stretch mode for the QS-MMA radical.

Table of Contents Graphic

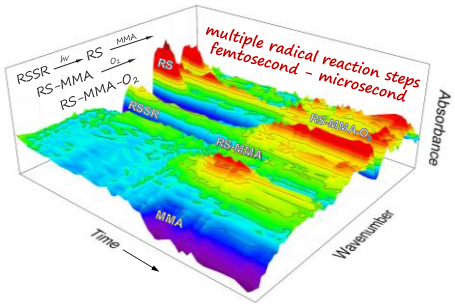

Multiple radical reaction steps have been observed in a continuous sequence with sub-picosecond to microsecond transient absorption spectroscopy.